Plasma-based N2 fixation into NOx : insights from modeling toward optimum yields and energy costs in a gliding arc plasmatron

Plasma-based N_2 fixation into NO_x: Insights from modeling toward optimum yields and energy costs in a gliding arc plasmatron

E. Vervloessem*[1], M. Aghaei*[2], F. Jardali*[3], N. Hafezkhiabani*[4], A. Bogaerts*[5]

**Research group PLASMANT, Department of Chemistry, University of Antwerp, Universiteitsplein 1, 2610 Antwerp, Belgium*

[1]*elise.vervloessem@uantwerpen.be*

[2]*maryam.aghaei@uantwerpen.be*

[3]*fatme.jardali@uantwerpen.be*

[4]*neda.hafezkhiabani@uantwerpen.be*

[5]*annemie.bogaerts@uantwerpen.be*

Abstract: *Plasma technology provides a sustainable, fossil-free method for N_2 fixation, i.e., the conversion of inert atmospheric N_2 into valuable substances, such as NO_x or ammonia. In this work, we present a novel gliding arc plasmatron at atmospheric pressure for NO_x production at different N_2/O_2 gas feed ratios, offering a promising NO_x yield of 1.5% with an energy cost of 3.6 MJ/mol NO_x produced. To explain the underlying mechanisms, we present a chemical kinetics model, validated by experiments, which provides insight into the NO_x formation pathways and into the ambivalent role of the vibrational kinetics. This allows us to pinpoint the factors limiting the yield and energy cost, which can help to further improve the process.*

Keywords: Plasma-based N_2 fixation; gliding arc plasmatron; NO_x formation, energy cost; chemical kinetics modeling; nitrogen fixation; plasma modeling; vibrational kinetics

INTRODUCTION

Nitrogen (N_2) is an essential building block for all living organisms. Global N_2 is predominantly present in the form of chemically-inert atmospheric N_2, which makes up 78% of the air. In order to make it accessible for living organisms, N_2 has to be transformed to a reactive form, such as ammonia (NH_3) or nitrogen oxides (NO_x), by its reaction with H_2 or O_2 gas, in a process called N_2 fixation (NF).[1] This can be achieved through naturally occurring, high energy-consuming processes (abiotic) and through specialized organisms (biotic)[2–4]. The growing population however requires more fixed N_2 than the Earth can provide. To this end, the Haber-Bosch (HB) process for NH_3 synthesis was developed, supporting 40% of the world population[1]. Nevertheless, this industrial NF process requires 1% of the total energy production worldwide and 3 – 5% of the globally produced natural gas, and it emits more than 300 million tons of CO_2 per year[2,5,6]**.** Owing to the increasing demand for fertilizers, as well as to the high energy cost and environmental impacts of the current industrial HB process, considerable efforts are devoted to provide alternative and greener approaches on an industrial scale.[7–13]

Among others, plasma technology is a promising method[7,11,14,15]. A plasma reactor is powered by electricity, and can be easily turned on/off, so it can be integrated with fluctuating renewable electricity sources[5,7]. Moreover, it has no economy of scale, so it can be used on site at a variable scale, producing fertilizers when needed, by using available sustainable energy sources[8,14,15]. Furthermore, it offers a safe and cheap process, as it operates at ambient pressure and temperature, hence at milder conditions than the HB process. The theoretical energy cost of plasma-based NF is 0.2 MJ/mol NO_x, i.e., 2.5 times lower than the HB process[16]. In plasma, the applied electric energy is predominantly transferred to the electrons, which activate the gas molecules by

electron impact excitation, ionization and dissociation reactions. Hence, the gas does not have to be heated as a whole for the conversion process, thereby limiting the energy cost[14,17,18].

Special interest is given to NO_x production from air, as a low-cost and abundant raw material [8,11,14,15], compared to NH_3 production, which typically requires expensive H_2 gas in the mixture.

Several thermal and non-thermal plasma sources have been applied for NO_x formation (see Table S.1 in the Supporting Information (SI) for details). Thermal plasmas, like radio-frequency (RF)[19], jet[20,21], laser produced[22], and arc[12,19] plasmas, typically yield 1 – 6.5% NO_x production, but at a high energy cost (2.41 – 1638 MJ/mol), because the energy in a thermal system is distributed over all degrees of freedom. The best results for thermal plasmas were obtained for an electric arc, yielding 1 – 2% NO without[12] (Birkeland-Eyde process) and 4.7% with water injection,[19] at an energy cost of 2.41 and 3.50 MJ/mol NO, respectively. For non-thermal plasmas, the most promising results have been obtained in microwave (MW) plasmas at reduced pressure, because of the dominant role of the energetically favourable vibrational-induced dissociation of N_2[15]. A yield of 6% NO at an energy cost of 0.84 MJ/mol NO has been reported in a MW plasma at 66 mbar, with MoO_3 catalyst[23]. A pulsed MW plasma at reduced pressure without catalyst performed even better, with the same yield but an energy cost of only 0.60 MJ/mol NO[24]. The best yield (14% NO) and energy cost (0.30 MJ/mol NO) reported in literature so far, were for a MW plasma at reduced pressure and a magnetic field[25]. However, these results have not yet been reproduced since they were reported. Other non-thermal plasmas reported in literature include a dielectric barrier discharge (DBD) with $\gamma - Al_2O_3$ catalyst, yielding 0.5% NO_x at 18 MJ/mol NO_x[26], a shielded sliding discharge, producing 0.1% NO_x at 15.4 MJ/mol NO_x[27], and a pulsed milliscale gliding arc (GA) at atmospheric pressure, producing 2% NO_x at a cost of 2.8 MJ/mol NO_x[8,28]. Just like in a MW plasma, a GA plasma promotes vibrational-induced

dissociation, resulting in a lower energy cost,[11,15] although this mechanism is not fully exploited at atmospheric pressure, explaining the higher energy cost than for the MW plasmas at reduced pressure.

In this paper, we present NO_x production in a novel reverse vortex flow gliding arc plasmatron (GAP), developed at Drexel University.[29] This novel type of GA plasma is promising for gas conversion at atmospheric pressure, as demonstrated already for CO_2 conversion in pure CO_2[30] and in a $CO_2 – N_2$ gas mixture[31], as well as for dry reforming of methane[32], but it has not yet been applied for NO_x formation in a $N_2 – O_2$ gas mixture. To better understand and improve the GAP for gas conversion, the underlying mechanisms have been studied, both computationally[33–35] and experimentally,[36,37] but only in argon, pure CO_2 and pure N_2, while the chemistry has also been modelled in $CO_2 – CH_4$[32] and $CO_2 – N_2$ [31] gas mixtures.

In order to elucidate the underlying mechanisms in a N2 – O_2 gas mixture in the GAP reactor, we combine our experiments with a zero-dimensional (0D) chemical kinetics model. To our knowledge, such a comprehensive computational and experimental study of NO_x formation in a GAP has never been performed. Even more, only a few papers have studied the underlying mechanisms of plasma-based NO_x formation in general.[11,31] The present study is therefore important to elucidate plasma-based N_2 fixation, giving us more insight in the chemistry to improve this process.

MATERIALS AND METHODS

Experimental setup

The experiments were performed with a novel type of GA plasma, called gliding arc plasmatron (GAP) (Figure 1), as developed by Nunnally et al.[29]**.** In a classical GA reactor, an arc discharge is created between two electrodes by applying a potential difference. Subsequently, this arc glides

along the electrodes dragged by a gas flow. The GAP, on the other hand, has a very different design. It is a cylindrical GA reactor in which the gas flows in the reactor through tangential inlets, creating a vortex, and an arc is formed between the reactor body (cathode potential) and outlet (anode). A schematic drawing of the GAP is illustrated in Figure 1. In our work, the outlet (anode) diameter (7.08 mm) is smaller than the reactor body (cathode) diameter (17.50 mm), so the gas is first forced to move upwards in the reactor in a forward vortex flow (FVF) (full black spiral in Figure 1). While the gas is moving , it loses rotational speed due to friction and inertia, and when it reaches the top part of the reactor, it moves down in a smaller reverse vortex flow (RVF) to the bottom where it can leave the reactor (dashed black spiral in Figure 1). This RVF surrounded by the FVF stabilizes the arc plasma in the centre. This novel design results in a better thermal insulation, which reduces heat loss and prolongs the lifetime of the electrodes.[38,39] A diagram of the entire experimental system including a photo is shown in SI Figure S.1.

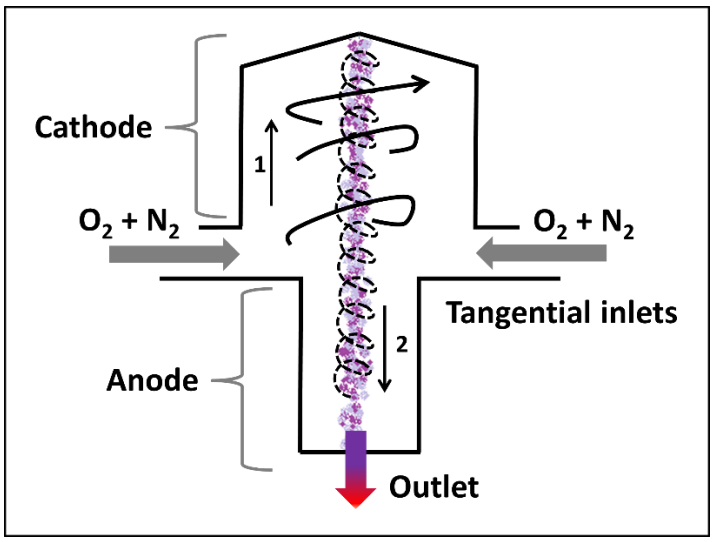

Figure 1 Schematic illustration of the GAP in reverse vortex flow configuration. Both the forward and reverse vortex flows are indicated (with full and dashed spirals, and numbers 1 and 2, respectively).

This vortex flow configuration stabilizes the plasma arc (indicated in purple) in the centre of the reactor, while the reverse gas flow passes through the plasma.

The reactor was powered by a DC power supply (APS-Advanced Plasma Solutions). The plasma voltage and current were measured by a high-voltage probe (Tektronix P6015A) and a current sense resistor of 6 Ohm, respectively. The electrical signals were sampled by a two-channel digital storage oscilloscope (Tektronix TDS2012C) and the current was varied between 0.2 and 0.4 A.

The output gas composition was analysed online by a mass spectrometer (Hiden Analytical Limited, QGA Pro v1.6). The mass spectrometer was calibrated separately with a mixture of 867 ppm NO_2 in He and 976 ppm NO in He. For both NO and NO_2, a response factor was calculated and used to determine the concentration of the detected products, i.e., NO and NO_2. The EC was calculated using Equation (1).

$$\mathrm{EC_{NO_x}}[\mathrm{MJ \cdot mol^{-1}}] = \frac{\text{Power [W]}}{\text{moles of } \mathrm{NO_x} \text{ produced per second } [\mathrm{mol \cdot s^{-1}}]} \cdot \frac{1}{10^6 \left[\frac{\mathrm{J}}{\mathrm{MJ}}\right]} \quad (1)$$

0D Model

We developed a zero-dimensional (0D) chemical kinetics model within the code ZDPlasKin[40], to describe the conversion of N_2 into NO_x in our GAP reactor. Such a model is most convenient for describing a complex chemistry. A set of continuity equations (see section 3 in the SI) is numerically solved for all individual species included in the model (see Table S.2 in the SI), in order to obtain the species densities as a function of time. Since the plasma is confined in the inner vortex of the gas flow, the plasma can be considered uniform and we can assume a constant power density applied to the gas during its residence time in the plasma. This is convenient for the 0D model, which does not include spatial variations or transport. However, the calculated temporal dependence of the species densities can be transformed into a spatial dependence through the reactor by means of

the gas flow rate[41,42] (see Figure S.2b in the SI). The arc plasma column is thus considered as a plug flow reactor, where the plasma characteristics vary as a function of distance travelled by the gas within a certain residence time.

Vibrational excitation of N_2 is promoted in the GAP and is advantageous for more energy-efficient dissociation of N_2, because it can help to overcome the reaction energy barrier of the Zeldovich mechanism.[17,41] Therefore, special attention is given to the vibrational levels: 24 vibrational levels for N_2 and 15 levels for O_2 were implemented in the model. The species taken into account in the model are listed in Table S.2 in the SI. This includes neutral molecules in the ground, vibrationally and electronically excited states, various radicals, positive and negative ions, and electrons. All reactions with their reaction rate constants that are taken into account in the model are listed in section 9 of the SI.

RESULTS AND DISCUSSION

NO_x yield and energy cost

Figure 2a shows the experimental and calculated NO (blue) and NO_2 (red) yields as a function of N_2 fraction in the gas mixture, for a gas flow rate of 10 L min^{-1} and a pressure of 1.25 bar. All experiments were repeated three times to determine the measurement uncertainty. The experimental NO yield increases upon increasing N_2 fraction, until it reaches a maximum value of 1.4% at 80% N_2, after which the yield drops slightly. Interestingly, the highest yield is obtained for a gas composition very similar to the composition of air (78% N_2). Therefore, N_2 – O_2 gas separation before the reactor can be avoided, reducing the costs for industrial applications.

The calculated NO yield (dashed blue curve) follows the experimental trend, but shows a maximum

at 60% N_2. Indeed, according to the model, both N_2 and O_2 molecules must be present at almost equal amounts for the highest NO production. Still, the highest yield is reached at slightly higher N_2 than O_2 fractions, as in the experiments, but the parabolic trend is more pronounced than in the experiments. This results in a calculated NO yield at 40 – 60% N_2 to be slightly above the range of the experimental error bars. The reason for this discrepancy is not yet fully understood, but might be attributed to certain reaction rates that can be slightly over– and/or underestimated in our model. However, we did not want to tune our rate coefficients to reach an exact agreement without scientific basis. Nevertheless, in general, the calculated results show good agreement with the experiments, keeping in mind the complex chemistry and the approximations inherent to a 0D model (see above and in the SI).

The trends of the calculated and experimental NO_2 yields are in very good agreement. The calculated NO_2 yield, however, is underestimated by a factor two. Considering the complexity of the chemistry included in the model, it is reasonable to conclude that our model adequately describes the plasma chemistry, in spite of the above-mentioned discrepancies, and can therefore be used to elucidate the underlying mechanisms in a $N_2 – O_2$ gas mixture in the GAP reactor, as will be presented later in this paper. The total NO_x yield, i.e. yield of NO + NO_2, and energy cost (EC) for the formation of NO_x obtained from the experiments, are plotted in Figure 2 (b-c, solid lines) and are compared to the simulation results (dashed lines). The total NO_x yield rises upon higher N_2 fractions, reaching a maximum of 1.5%. Because more or less the same amount of power was applied in the entire range (varying between 365 and 458 W; see SI Table S.3, this yields a lower EC at higher N_2 fractions (see equation (1) above), with a minimum value of 3.6 MJ/mol NO_x at 70-80% N_2 (Figure 2c). Note that the value of the power, needed to calculate the EC, was obtained as the average of at least 100 voltage–current (V–I) cycles. The calculated EC shows good agreement with the experimental

results, except for fractions below 40% N_2, where the calculated NO_x yield is underestimated (Figure 2b).

Note that we also checked for other N_xO_y species in our experiments, such as N_2O and N_2O_4, but their concentrations were below the detection limit of the MS. This was confirmed by the 0D model, because the calculated yields were 3.2 x 10^{-4} % (density of 6.58 x 10^{13} cm^{-3}) or lower for N_2O , and below 3.2 x 10^{-11} % (density of 5.47 x 10^5 cm^{-3}) for N_2O_4, for all feed ratios. The same was true for other N_xO_y species in our model, i.e., NO_3, N_2O_5 and N_2O_3. The exact densities are listed in Table S.7 in the SI.

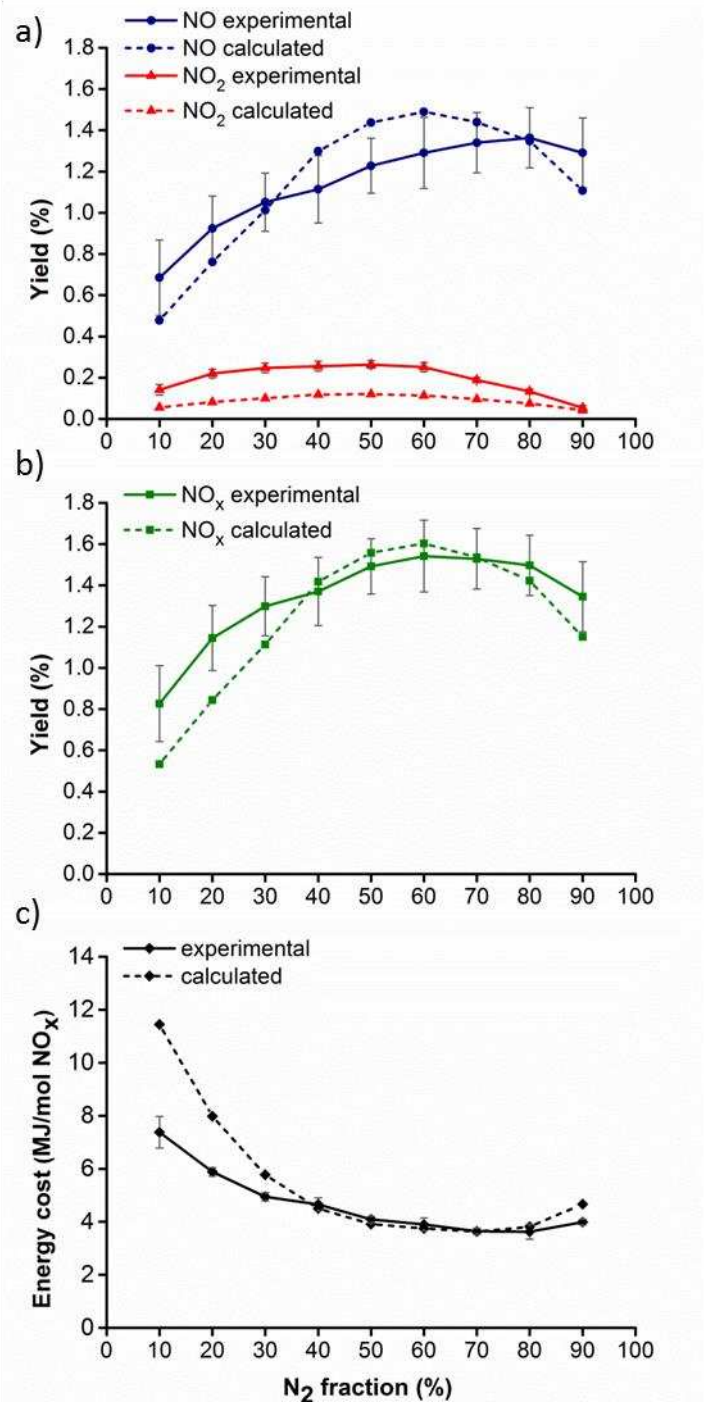

Figure 2 *Experimental (solid lines) and calculated (dashed lines) yield of NO (blue) and NO_2 (red) (a), total NO_x yield (b), and energy cost (c), as a function of* N_2 *fraction in the feed gas, for a gas flow rate of 10 L min^{-1}, a pressure of 1.25 bar and a power ranging from 365 to 458 W (slightly varying for different gas composition; see supporting information (SI) Table S.3).*

Figure 3 shows the measured and calculated NO and NO_2 yields as a function of the flow rate. The NO and (especially) NO_2 yield drop upon higher flow rate, due to the shorter residence time, as expected. In this paper we selected a flow rate of 10 L min^{-1} (see Figure 2), because it showed the highest total NO_x yield in the range of 8 – 30 L min^{-1} and because the ignited plasma was stable for all feed compositions reported (which was not the case at 8 L min^{-1}). The calculated yields are in reasonable agreement with the experimental values. The trend, however, does show some discrepancies, especially for the NO_2 yield. This shows the limitations of a 0D model in capturing the flow effects, which is logical, as the flow enters tangentially in our GAP reactor, so the flow path lines are essentially 3D. It is clear from Figure 2 that our model is much more capable at capturing changes in feed compositions.

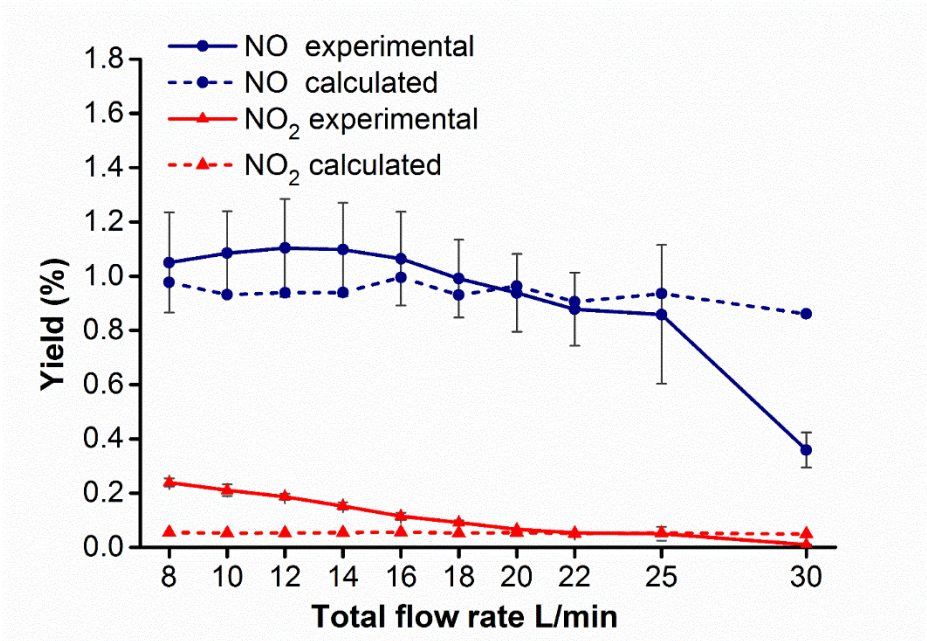

Figure 3 Experimental (solid lines) and calculated (dashed lines) yield of NO (blue) and NO_2 (red) as a function of the flow rate, at a power ranging from 364 to 548 W (slightly varying for different flow rates; see Supporting Information (SI) Table S.3).

Comparison with different plasma sources applied for NO_x formation

In Table S.1 in the SI, we compare our results with other plasma discharges used for NO_x production. The optimum NO_x yield of 1.5%, obtained in our GAP, is close to the yields obtained by the original Birkeland-Eyde process[12] and the pulsed milliscale GA reactor[28]. Other reported plasma reactors produce lower NO_x yields [26,27], except for MW plasmas, showing clearly higher yields, between 6 and 14% [23–25], but these results were all obtained at reduced pressures, compared to the atmospheric pressure in our GAP. With increasing pressure, the gas number density increases, so the vibrational-translational energy losses become more pronounced, lowering the vibrational populations of the N_2 molecules, thus limiting the most efficient NO_x formation path (see Underlying mechanisms for NO an NO_2 formation in the GAP below). Another important factor affecting the NO_x yield in the GAP is the limited fraction of gas molecules that pass through the arc plasma, i.e., around 15%, as demonstrated by higher dimensional modeling[33]. Indeed, if not 15% but 100% of the gas would be treated, the NO yield would reach a maximum of 8.2%. This will be discussed further below.

Our energy cost of 3.6 MJ/mol NO_x is also similar to the Birkeland-Eyde process and the pulsed milliscale GA, and much better than some other reported set-ups, but worse than the reduced pressure MW plasmas. However, working at reduced pressure requires pumping, which makes it less viable for industrial applications, and this cost should be accounted for in the calculation of the total energy cost of the process, which was not the case for the values reported in ref [23–25]. A comparison between plasma at atmospheric and reduced pressure is thus not a fair comparison. In addition, as mentioned in the Introduction, they have not been reproduced since then.

It is also worth to note that the energy cost calculated in our GAP, when only accounting for the conversion in the arc itself (i.e., considering that all gas molecules would be able to pass through the arc) would be as low as 0.5 MJ/mol NO_x. This would approach the thermodynamic minimal energy cost for plasma-based NO_x formation of 0.2 MJ/mol NO_x [16]. Unfortunately, the actual energy cost is much higher, because not all the gas molecules pass through the arc. Hence, this illustrates that there is still some room for improvement, by modifying the reactor design so that more gas can pass through the arc plasma.

The various plasma sources listed in Table S.1 are all different in structure, geometry and excitation modes, and they potentially have different chemical reaction pathways for NO_x production. Therefore, Pei et al. proposed a dimensionless parameter (χ) to compare different plasma set-ups[42]. How our GAP performs when comparing the different plasma set-ups using this parameter is discussed in the SI. The minimum energy cost in GJ/tN in our GAP is 257 GJ/tN. If we would add this data point to the figure in ref.[42] (see Figure S.3 in SI), our EC is in the range of what is predicted by the linear dependency between EC and χ.

Comparison with thermal NO_x formation and the H-B process

Since the gas temperature in our GAP is relatively high compared to other plasmas used for NO_x production[5], i.e., around 3000 K, the question arises whether the NO_x formation process in our GAP is mainly based on thermal N_2 dissociation. The theoretical thermal yield can be calculated based on the chemical equilibrium composition, which is determined by finding the composition that minimises the Gibbs free energy [43,44]. At 3000 K, this results in a value of ca. 5.5% for a 50/50 N_2/O_2 mixture. Hence, the total NO_x yield (1.49%) at 50% N_2 in our GAP is lower than the calculated thermal yield at 3000 K, but this is mainly attributed to the fact that only 15% of the gas is treated by the arc. When we compare the NO_x yield at 50/50 N_2/O_2 obtained in the arc alone, i.e., 9.9%, this value

is higher than the thermal yield, and the EC is 0.5 MJ/mol NO_x vs. 2.1 MJ/mol NO_x for the pure thermal conversion. Indeed, the specific energy input (SEI) needed to achieve this conversion of N_2 in the GAP is significantly lower than for thermal NO_x formation (i.e., 0.59 vs 1.25 eV/molecule). This demonstrates that the NO_x production in the GAP proceeds in a more efficient way than only by thermal conversion, as we will illustrate below. At the same time, however, it indicates that the good performance is limited by the small amount of gas passing through the plasma arc. Hence, there is room for further improvement by modifying the design, which we plan in our future work (see also the section on: "How can the model help to improve the NO_x production and energy cost?").

Nonetheless, it should be noted that our GAP is roughly a thermal plasma, as the VDFs are near Boltzmann-distributed determined by the gas temperature. However, as shown by our investigation of the VDFs and the N_2/O_2 VV exchanges (below) and our comparison with thermal conversion (above), the vibrational kinetics do play a crucial role. Importantly, compared to a classical thermal reactor, it is generally easier to reach higher temperatures, as the vortex flow isolates the hot plasma from the walls.

Finally, our discussion above indicates that the yield and energy cost reached in our GAP are not yet competitive with the current industrial Haber-Bosch (HB) process. However, we should probably not benchmark with the HB process, which operates at large scale and was optimized for more than 100 years. Plasma-based N_2 conversion has other environmental and economic advantages to offer, compared to a large scale, continuous, and fossil fuel dependent industrial process. Indeed, small, decentralized plasma plants could independently provide fixed N_2 on-site using the surrounding air as feed-stock.

Underlying mechanisms for NO an NO_2 formation in the GAP

Formation of N and O atoms in the GAP

To better understand the underlying chemistry in the GAP, we plot in Figure 4 the number densities of NO, NO_2, O and N atoms as a function of time for three different feed compositions. The densities of N_2O_4, N_2O, N_2O_5 and N_2O_3 are negligible throughout the whole residence time.

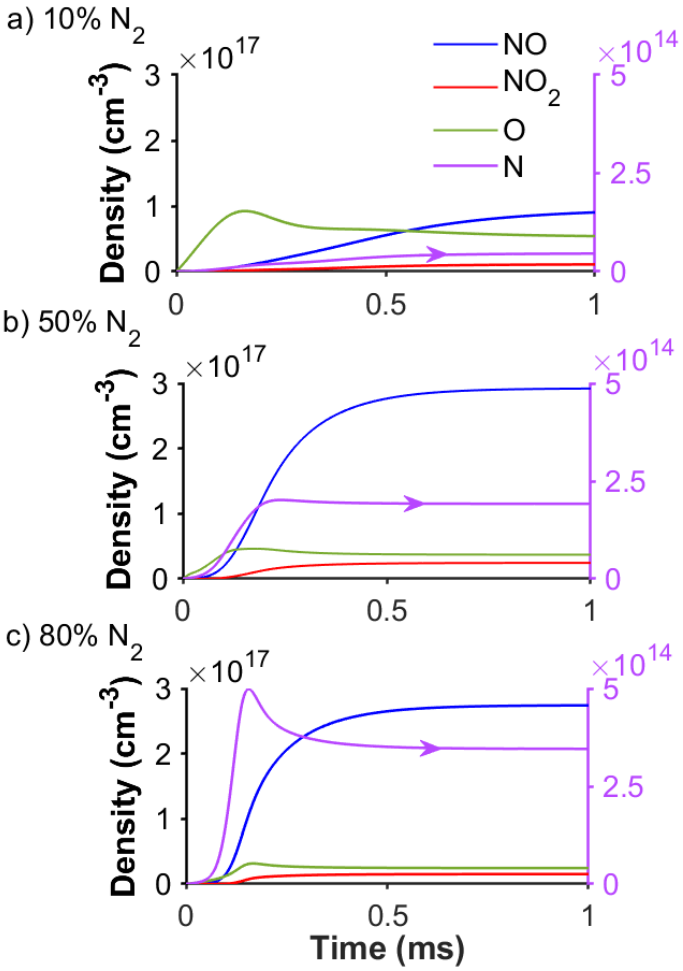

Figure 4 Calculated number densities of NO, NO_2, O and N as a function of the residence time in the plasma for 10 (a), 50 (b) and 80% N_2 (c), at 1.25 bar, 10 L min^{-1} and the power values listed in Table S.3 in the SI. For clarity we only plot the densities up to steady state (1 ms), while the whole residence time is 15 ms. Note that the N atoms are plotted on the right y-axis, as their density is up to three orders of magnitude lower.

For all feed compositions, steady state is reached before 1 ms. For clarity only 1 ms is shown, but the entire residence time is 15 ms. Reaction analysis shows that the pathway for NO and NO_2 formation is the same for all feed compositions, as will be discussed in detail in the following two sections. This pathway is initiated by N and O atoms (see below). Both atoms are formed upon dissocation of N_2 and O_2 molecules (see below), and reach their maximum before 0.2 ms (with the exception of N at 10% N_2), after which it drops to reach steady-state values. As is clear from Figure 4, the O atom density is two-three orders of magnitude larger than the N atom density, because of much easier dissociation of O_2 than N_2 molecules (bond dissociation energy of 5.15 eV vs 9.79 eV). Both N and O atoms are consumed upon collision with O_2, N_2, NO and NO_2 (reactions N1 – N4 in Table 2 below). The production and consumption of O atoms is nearly the same for all feed compositions, while the production of N atoms increases upon increasing N_2 fraction. Reaction analysis can explain this behaviour: (1) The N atoms are mainly (99%) produced through direct electron impact dissociation of N_2(g/v), so their production is directly correlated to the N_2 fraction in the feed. (2) The O atoms, on the other hand, are mainly (99%) produced through two separate mechanisms, and depending on the feed ratio one mechanism dominates over the other, i.e., (a) direct electron impact dissociation of O_2(g/v), and (b) dissociation upon collision with electronically excited N_2 molecules ($O_2\ (g/v) + N_2\ (E) \rightarrow\ N_2 +\ O + O$). Mechanism (b) is the main (80%) production channel at 80% N_2 in the feed, while mechanism (a) is the main (90%) production channel at 10 % N_2. Different O production channels are thus promoted at different feed ratios, while the production of N atoms solely depends on the availability of N_2(g/v). This shows that the production of N atoms is clearly the limiting factor in the production of NO_x. Note that the N and O atom densities are constant in time after reaching steady state, but at the end of the reactor, i.e., outside

the plasma, their densities drop rapidly, because they are not produced any further through electron impact dissociation (or collisions with $N_2(E)$ in the case of the O atoms).

Formation and destruction mechanisms of NO and NO_2 as a function of the N_2/O_2 ratio in the feed. To gain further insight into the NO_x formation (and loss) mechanisms in the GAP, we performed a detailed reaction analysis for different fractions of N_2 in the feed gas. We calculated the time- and space-averaged reaction rate for each formation and loss process of both NO and NO_2, and their contribution to the total formation/loss of both species. The detailed analysis, i.e., formation and loss rates for the various reactions, as a function of N_2/O_2 ratio in the mixture, is presented in the SI (Figure S.4). Table 1 shows the important processes with the highest contributions to the formation and loss of NO and NO_2 for an 80/20 N_2/O_2 gas feed ratio, as an example.

Table 1 Main reactions for the formation and loss of NO (F, L) and NO_2 (f, l) and their relative contributions, at an 80/20 N_2/O_2 ratio. Reactions annotated with an asterisk are not important in N_2/O_2 mixtures, but are listed for the sake of completeness, as they become significant upon the addition of ozone, as will be explained below. (g) and (v) denote the molecules in the ground state vs vibrational levels, respectively.

Reaction	Contribution [%]		Reaction	Contribution [%]	
Main reactions for NO formation (F)			Main reactions for NO_2 formation (f)		
$NO_2 + M \rightarrow NO + O + M$	90.7	F1	$NO + O\ (+M) \rightarrow NO_2\ (+M)$	96.1	f1=L1
$O + NO_2 \rightarrow NO + O_2$	2.5	F2	$NO + O_2(v) \rightarrow NO_2 + O$	2.5	f2=L2
$O + N_2(g) \rightarrow NO + N$	0.07	F3	$NO + O_2(g) \rightarrow NO_2 + O$	1.9	f3=L3
$O + N_2(v) \rightarrow NO + N$	7.8	F4	$NO + NO_3 \rightarrow NO_2 + NO_2$	1.1	f4
$N + O_2(g) \rightarrow NO + O$	0.8	F5	$NO + NO + O_2(g) \rightarrow NO_2 + NO_2 *$	± 0	f5
$N + O_2(v) \rightarrow NO + O$	1.1	F6	$NO + NO + O_2(v) \rightarrow NO_2 + NO_2 *$	± 0	f6
$NO_2 + NO_2 \rightarrow NO + NO + O_2*$	± 0	F7			
Main reactions for NO loss (L)			Main reactions for NO_2 loss (l)		
$NO + O\ (+M) \rightarrow NO_2\ (+M)$	91.0	L1	$NO_2 + M \rightarrow NO + O + M$	96.0	l1=F1
$NO + O_2(v) \rightarrow O + NO_2$	2.4	L2	$O + NO_2 \rightarrow NO + O_2$	2.7	l2=F2
$NO + O_2(g) \rightarrow O + NO_2$	0.2	L3	$NO_2 + NO_2 \rightarrow NO_3 + NO$	1.2	l3
$O + NO \rightarrow N + O_2$	1.9	L4	$NO_2 + NO_2 \rightarrow NO + NO + O_2 *$	± 0	l4
$N + NO \rightarrow O + N_2$	4.0	L5	$*$ reactions that become significant upon the addition of ozone (see section below).		
$NO + NO + O_2(g) \rightarrow NO_2 + NO_2 *$	± 0	L6			
$NO + NO + O_2(v) \rightarrow NO_2 + NO_2 *$	± 0	L7			

As is clear from Table 1, both for NO (and NO_2) formation and loss, the main contribution comes from reactions F1 (f1) and L1 (l1), followed by F2 (f2) and L2 (l2). However, these reactions only lead to the conversion of NO into NO_2, and vice versa, but they do not represent the net formation of NO (and NO_2) from N_2 and O_2. The latter is initiated by the reactions comprising the so-called Zeldovich mechanism (see below; reactions F2 – F6). Although these reactions have a contribution

an order of magnitude lower, they are crucial for the formation of NO (see below). The same applies to the NO loss reactions (L4 and L5). Finally, f4 and l3 play a minor role in the formation and loss of NO_2.

Because it is clear that the main formation processes of NO are the main loss processes of NO_2, and vice versa, and because the formation reactions can be counteracted by their reverse reactions, we have to look at the net rate of these reactions (i.e., rate of forward minus reverse reaction). The reaction scheme in Figure 5 visualizes the reaction pathways for the formation and loss of NO and NO_2 for an 80/20 N_2/O_2 feed gas ratio, and Table 2 summarizes these processes.

Table 2 Main net NO and NO_2 formation or loss processes.

	Process	Reaction
N1	= F2 – (L2 + L3)	$NO_2 + O \rightarrow NO + O_2$
N2	= (F3 + F4) – L5	$N_2(g/v) + O \rightarrow NO + N$
N3	= (F5 + F6) – L4	$O_2(g/v) + N \rightarrow NO + O$
N4	= L1 – F1	$NO + O\ (+M) \rightarrow NO_2\ (+M)$
N5	= I3 – f4	$NO_2 + NO_2 \rightarrow NO + NO_3$

The Zeldovich mechanism: the initial and rate-limiting step in the formation of NO.

Initially, NO is formed through the Zeldovich mechanism (reaction N2 followed by N3, see Table 2, and indicated in red in Figure 5) promoted by vibrational excitation (green arrow lines in Figure 5). Indeed, in our GAP, like in other GA plasmas, the greatest fraction of the electron energy is transferred to vibrational excitation of the gas molecules (see also the next section below and section 8 in the SI), because the reduced electric field is in the range of 5 – 100 Td.[11] This vibrational

excitation facilitates the splitting of the strong triple bond of the N_2 molecule (≈ 10 eV). More than 98% of NO is formed through vibrationally excited N_2 molecules, indicating the importance of the vibrational chemistry.

The Zeldovich mechanism proceeds as follows: firstly, the strong triple bond of N_2 is broken through its reaction with an O atom, resulting in the formation of NO and N. As mentioned, this reaction is greatly facilitated by vibrational excitation of N_2 to overcome the high energy barrier of this reaction:

$$N_2(v) + O \rightarrow NO + N \qquad \text{(N2)}$$

Next, the N atom further reacts with vibrationally excited O_2 molecules, forming an O atom and a second NO molecule, and closing the reaction cycle:

$$O_2(v) + N \rightarrow NO + O \qquad \text{(N3)}$$

The N and O atoms are thus both produced and consumed in the Zeldovich mechanism, but their initial production happens through electron impact dissociation of N_2 and O_2, and for the O atoms also upon collision of O_2 with N_2(E), as explained in the section "Formation of N and O atoms in the GAP" above.

The net rates of the Zeldovich processes, i.e. N2 and N3, are plotted as a function of N_2 fraction in SI Figure S.4. Note that the rates of N1 and N4 are an order of magnitude higher, but they only convert NO into NO_2 and vice versa (right side of Figure 5: black arrow lines), but do not initiate the formation of NO. That is why we focus on the rates of N2 and N3. The net rate of N2 increases steadily with increasing N_2 fraction and reaches a maximum between 70 and 80% N_2. One would expect this maximum to be at equal amounts of N_2 and O_2, because the reaction requires both N_2(v) and an O atom. However, at O_2 fractions between 40 and 50%, the N_2(v) population is lower, due to

efficient VV exchanges between the O_2 and N_2 vibrationally excited molecules (green arrow lines in Figure 5; see detailed explanation in the next section below), which will reduce the rate of N2. The rate of process N3 is nearly independent from the gas composition. ~~, because both O_2(v) and N atoms are needed.~~ Indeed, at low N_2 fractions, the production of N atoms is low, while at high N_2 fraction, there is less O_2 available. Note that both O_2(v) (which is produced from O_2 molecules) and N atoms are needed for this reaction. Hence, at low N_2 fraction, the N atoms are the limiting factor, while at high N_2 fractions, the O_2 molecules are limiting, but overall, the effect is comparable, and explains why the rate of this process is nearly independent from the gas composition.

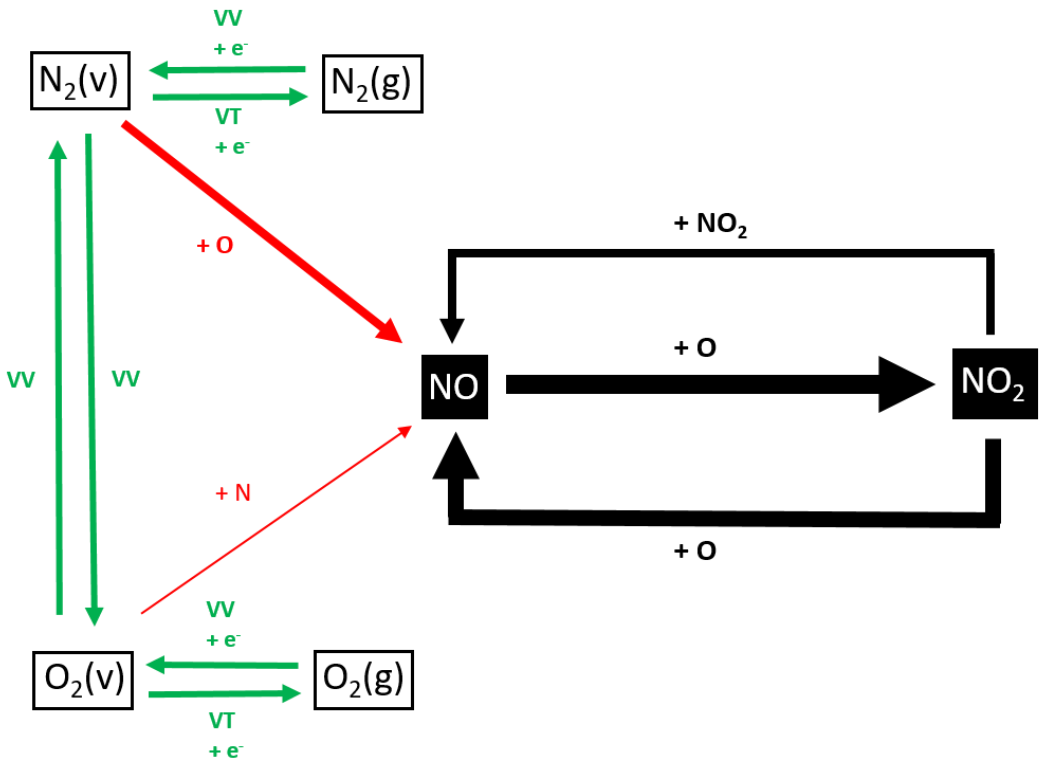

Figure 5 Reaction scheme to visualize the main reaction paths for NO_x synthesis. The thickness of the arrow lines corresponds to the importance of the reactions (net rate, i.e., forward minus backward reaction) for an 80/20 N_2/O_2 mixture at 1.25 bar, 10 L min^{-1} and 415 W. The two steps of the

Zeldovich mechanism are depicted in red, the vibrational-vibrational, vibrational-translational exchanges and electron impact reactions are in green.

The effect of O_2 on the VDF of N_2: the ambivalent role of the vibrational kinetics

It is clear from above that the vibrational kinetics are important for NO_x production in the GAP, so we want to investigate the vibrational populations in more detail. On the one hand, vibrational-induced dissociation is known to be the most energy-efficient pathway, because low-energy electrons populate the lowest vibrational levels by electron impact excitation, and gradually the higher levels are populated by vibrational-vibrational (VV) exchanges, i.e., so-called ladder climbing, until dissociation takes place from the highest vibrational levels. On the other hand, however, our simulations reveal the vibrational kinetics can also play a limiting role in the NO_x production. We call this the ambivalent role of the vibrational kinetics.

Vibrational-vibrational (VV) exchanges do not only take place between different N_2 molecules and between different O_2 molecules, but also upon collision between N_2 and O_2 molecules. As the O_2 vibrational levels are more easily depopulated, the VV exchange between N_2 and O_2 vibrationally excited molecules results in a depopulation of the N_2 vibrational levels, and in a net population of the O_2 vibrational levels. (For a detailed discussion see SI.) This is clear from Figure S.8 in the SI, showing the comparison of the VDFs of N_2 and O_2 with (full curves) and without (dashed curves) these VV exchanges. We plot the results for a 50/50 N_2/O_2 gas feed ratio, to illustrate most clearly the effect of these VV exchanges. If the $N_2 – O_2$ VV exchanges are taken into account, the vibrational levels of N_2 are less populated than when they are not included, while for O_2 the opposite is true. Thus, the O_2 vibrational levels depopulate the N_2 vibrational levels through $N_2 – O_2$ VV exchanges.

This process explains why the maximum in NO formation is reached at a N_2 fraction above 50%, while based on the stoichiometry it would be expected at equal fractions of N_2 and O_2. Indeed, at higher N_2 fractions, the depopulation of the N_2 vibrational levels (upon collision with O_2 molecules) is more limited and the vibrational ladder climbing, aiding the Zeldovich mechanism for NO formation (see above), is better promoted.

When these $N_2 - O_2$ VV exchanges are omitted in the model, the calculated yield is substantially higher (2.4% NO, vs. 1.4% NO when they are included) and the maximum is found at 50% N_2, as illustrated in Figure 6. From Figure 6 we can deduce that for the N_2/O_2 composition of air (78% N_2), the yield could be improved with 30%, while for a 50/50 N_2/O_2 feed ratio, the yield could even be doubled, if $N_2 - O_2$ VV exchanges could be avoided. We call this the ambivalent role of the vibrational kinetics in our GAP, i.e., the N_2 vibrational levels are beneficial for energy-efficient NO_x formation, but their effect is reduced by collisions with the O_2 vibrational levels. This is an important finding, which will be discussed further in the next section.

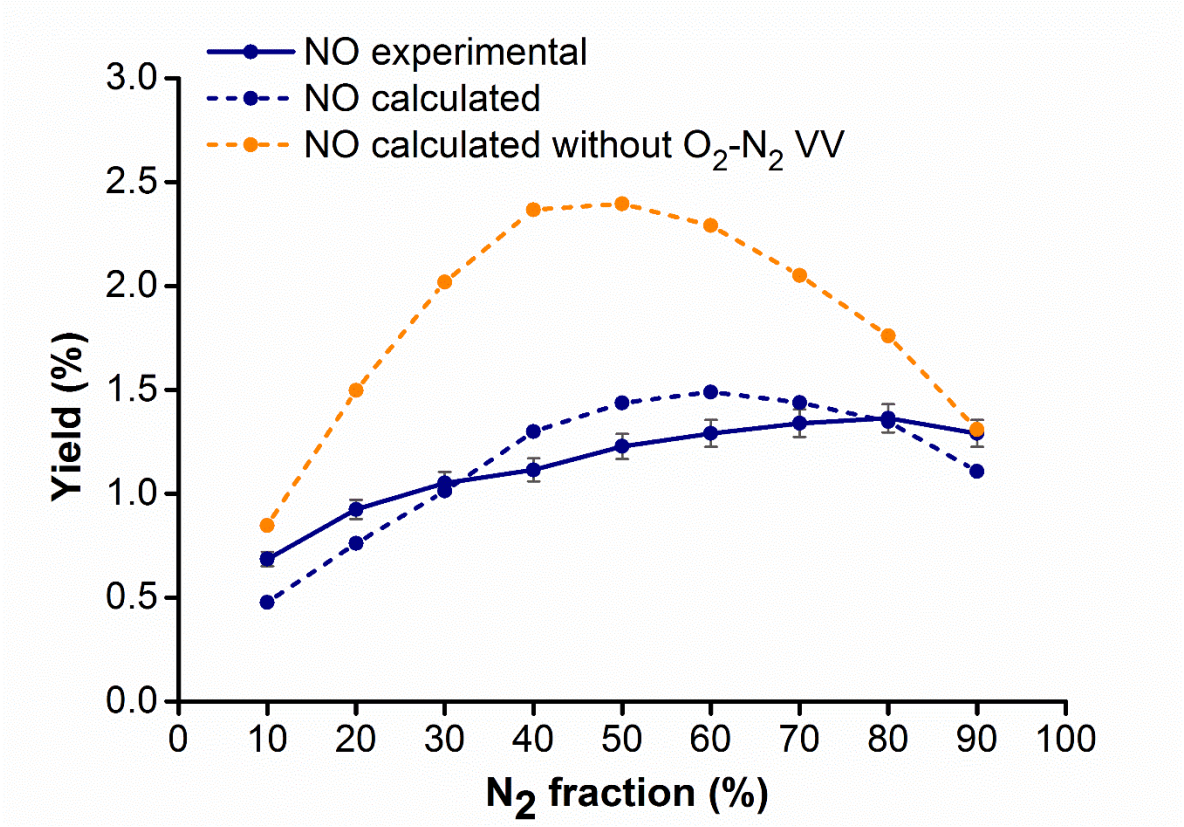

Figure 6 Experimental and calculated yield of NO (blue) compared to the calculated yield of NO without including $N_2 – O_2$ VV exchanges in the chemistry set (orange), as a function of N_2 fraction in the feed gas, at the same conditions as in Figure 2.

How can the model help to improve the NO_x production and energy cost?

It is clear that the limited gas fraction passing through the arc, the reverse reaction of the Zeldovich mechanism, and the $N_2 – O_2$ VV exchanges are the limiting factors in the NO_x production. We will now discuss how to overcome these hurdles.

First, as discussed previously, we believe the most notable improvement in yield and energy cost could be achieved if we could increase the fraction of gas that passes through the arc. Indeed, if all the gas would pass through the arc, our model predicts a NO_x yield of 9.9%, with an EC of 0.5 MJ/mol

NO_x, compared to the current values of 1.5% and 3.6 MJ/mol NO_x. We believe that decreasing the radius of one or more tangential inlets in order to create a higher flow velocity and more turbulence, would force more gas through the central arc. Additionally, increasing the plasma production and arc stability could be useful, and might be realized by changing the cathode design. Both approaches however need to be evaluated with fluid dynamics simulations and will be subject of our future work. While the ideal scenario, in which all the gas can pass through the arc, might be difficult to realize in our GAP, even after reactor design improvements, every modification that can increase this fraction above the current value of 15%, would improve the performance. With the knowledge we have now, we expect the yield to increase linearly with increasing fraction of gas passing through the arc.

Second, Figure 6 above illustrated that limiting the $N_2 – O_2$ VV exchanges could significantly improve the NO_x production. Indeed, without these VV exchanges, the NO_x yield would be twice as high, and the energy cost twice as low, for a 50/50 N_2/O_2 feed ratio. As the vibrational chemistry is complex, the way to achieve this is not straightforward. The aim would be to limit the vibrational depopulation mechanisms of O_2. In this way, there would be a sufficient amount of vibrationally excited O_2 present, so that the chemical equilibrium of the $N_2 – O_2$ VV exchanges is not forced in favour of N_2 (v) depopulation. Another possibility would be to consider O_2 mainly as O atom provider (for the first step of the Zeldovich mechanism; reaction N2). However, we still need O_2(v) for the second step (N3). An option could be to generate the O atoms separately from the main N_2/O_2 plasma, for example by preheating, leading to thermal O_2 dissociation and also vibrational population. However, this would need to be investigated in practice, as this heating will also affect the energy cost. An alternative option could be to put a plasma before the GAP, with in between an oxygen conducting tubular membrane that enables the species of interest, like O^{2-} ions, to reach the

main (i.e., GAP) plasma. Selectively transporting species of interest into plasma was recently used successfully in plasma-activated electrolysis for the cogeneration of NO and H_2 by Patel et al.[45] However, further research would be needed to evaluate this option here in practice, and to investigate whether the cost of such an additional step could be compensated by the improved performance.

It should be mentioned that the thermal energy for the NO_x formation is entirely provided by the GAP. In future work we will investigate heat recovery, i.e., using the heat released at the outlet for pre-heating the gas entering the plasma reactor, so that no plasma power must be wasted for heating the gas, and can immediately be used for the conversion process.

Finally, from the above reaction analysis, we conclude that the NO production (and hence the energy cost) could be further improved if the reverse reactions of the Zeldovich mechanism, i.e. L4 and L5 (see Table 2 above), could be reduced. These reactions, in which either an O or N atom reacts with NO, forming N + O_2, or O + N_2, compete with the propagation of the NO production mechanism and terminate this reaction chain. Our model reveals that excluding those reactions from the chemistry set enhances the NO_x yield by 10-fold (reaching 14% at equal N_2 and O_2 amounts) and reduces the EC, up to 0.44 kJ/mol NO_x. Removing O or N atoms from the plasma, e.g., by means of reversible sorption, would however not improve the Zeldovich mechanism, as the O and N atoms play a crucial role in both the forward and backward reactions. In theory, the backward reaction could be avoided by removing NO from the reaction mixture once it has been formed. Unfortunately, most of the NO_x separation processes available are destructive, i.e. for the purification of exhaust gases[46,47]. Molecular sieves[48,49] and wet scrubbing[50] would be suitable methods to extract the produced NO_x after the GAP reactor, but we are not aware of methods that

can withstand the high temperature in the arc (~ 3000 K) and operate on a ms timescale, in order to reversibly ad- or absorb NO in the plasma itself.

If we cannot remove NO itself with current technologies, an alternative could be to convert NO into NO_2, resulting in the desired equilibrium shift towards NO formation, namely a rate increase for reactions F3 – F6 and a decrease for L4 and L5 (see Table 2). An option to realize this would be the addition of O_3 to the feed gas. The hypothesis is that O_3 increases the conversion of NO to NO_2, thus removing NO in this way from the reaction mixture.

To investigate this option, we performed simulations for air diluted with 0 – 30% O_3. Note that when only N_2 and O_2 are used as feed gas, the production of O_3 is found to be negligible (with a calculated yield below 3.2×10^{-5} %, according to our model) for all feed compositions. This suggests that roughly no O_3 is formed in the plasma, so it cannot help the conversion of NO to NO_2 after the plasma. Figure 7 shows the calculated NO (blue) and NO_2 (red) yield as a function of the O_3 fraction in the feed, at 10 L min^{-1} and 400 W. The yield clearly rises to 1.71 and 0.16%, for NO and NO_2, respectively, at 30% O_3, compared to 1.23 and 0.007% in pure air. This results in a drop in EC from 3.8 MJ/mol NO_x for 0% O_3, to 3.1 MJ/mol NO_x for 30% O_3.

In SI Figure S.5, we plot the net rate of the main NO formation reactions as a function of the O_3 fraction in the feed. We can conclude that the rise in NO_x yield is mostly attributed to the more efficient formation of O atoms. O_3 splits almost immediately upon collision with any neutral species, resulting in O_2 and O atoms. While the higher O_2 fraction upon O_3 addition would decrease the NO_x yield, as shown in Figure 2 (due to $N_2 – O_2$ VV exchanges), it appears that the positive effect of having more O atoms is more significant. However, the rise in O atom density does not significantly influence the Zeldovich mechanism (processes N2 and N3), as both the back and forward reactions

depend on the O_2 or O concentration. The largest effect can be seen in the conversion of NO to NO_2 (N4); see Figure S.5 in SI (loss process of NO). Also the rate of the reverse process (N1: conversion of NO_2 into NO) rises upon increasing O_3 fraction, but the effect on N4 is more pronounced, i.e., more NO is converted into NO_2. Hence, this could help to reduce the back reactions of the Zeldovich mechanism (loss of NO upon reaction with N or O atoms), resulting in a net increase in NO and NO_2 production.

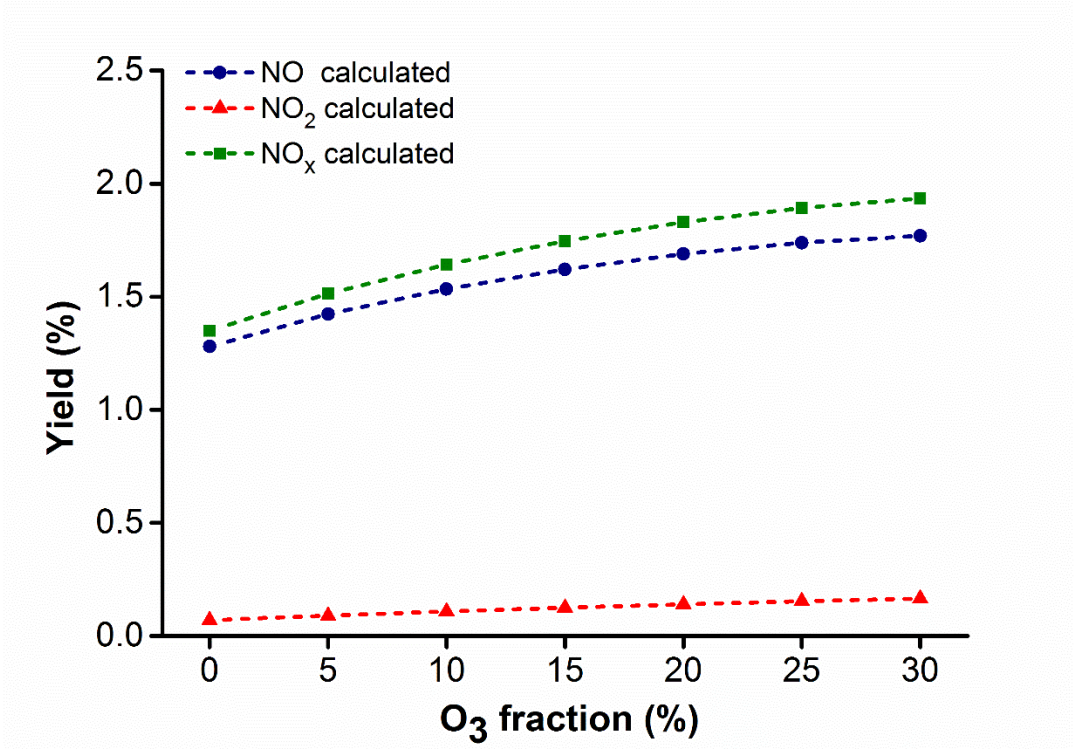

Figure 7 Calculated yield of NO (blue), NO_2 (red) and total NO_x (green) at 0 – 30% O_3 (dilution of air) at 10 L min^{-1} and 369 W.

CONCLUSIONS

We explored the performance of a novel type of GA plasma, called gliding arc plasmatron (GAP), for NO_x formation at different N_2/O_2 feed ratios and different inlet flow rates, by means of experiments and modeling. The highest yield of 1.5% NO_x with an energy cost of 3.6 MJ/mol NO_x was obtained

at 10 L min^{-1}, around 70/30 feed ratio of N_2/O_2, which is close to the composition of air. Our results are comparable to other results reported for N_2 fixation in plasma reactors[15]. In addition, we developed a plasma chemical kinetics model, validated by experiments, that provides insights into the underlying chemistry, which can help to identify the processes that limit the NO_x production.

Our study reveals that the vibrational excitation of N_2 can help to overcome the high energy barrier for N_2 dissociation. Indeed, NO is formed through the Zeldovich mechanism, which is stimulated by vibrational excitation: $O + N_2(v) \rightarrow NO + O$. This energy-efficient pathway explains the low energy cost for NO_x synthesis in the GAP. However, our model also indicates that the effective use of N_2 vibrational levels is limited by depopulation upon collision with O_2 vibrational levels, i.e., so-called $N_2 - O_2$ VV exchanges. This demonstrates the ambivalent role of the vibrational kinetics in the energy-efficient NO_x formation in our GAP: the N_2 vibrational levels are beneficial, but the O_2 vibrational levels reduce this efficiency. Suppressing these VV exchanges would double the NO_x yield for a 50/50 N_2/O_2 feed ratio and increase it with 30% for an 80/20 N_2/O_2 ratio (which corresponds to air).

It should be noted that our GAP is roughly a thermal plasma, as the VDFs are near Boltzmann-distributed determined by the gas temperature. However, compared to a classical thermal reactor, it should be easier to reach higher temperatures, as the vortex flow isolates the hot plasma from the walls.

From our model, we can also conclude that it is important to operate at conditions at which the reverse reactions of the Zeldovich mechanism are suppressed ($NO + O \rightarrow N + O_2$ and NO $+N \rightarrow O + N_2$), as these processes limit the NO_x formation. In theory, this could be achieved by constantly removing NO from the reaction mixture, but this might not be straightforward in practice, given the

high temperature in the GAP. We suggest that the conversion of NO into NO_2 could be helpful, and we discussed the option of adding O_3 to the air feed gas, as a possible way of realizing this. Indeed, our model reveals that the addition of 30% O_3 enhances the total NO_x yield from 1.30% to 1.87%, with a drop in energy cost from 3.8 to 3.1 MJ/mol NO_x, which is due to the efficient formation of O atoms, enhancing the conversion of NO into NO_2.

Finally, we assert that the NO_x yield and energy cost could be drastically improved in our GAP by enlarging the fraction of gas passing through the arc, which is now limited to 15%, as revealed by fluid dynamics simulations. Our calculations predict that, if all the gas could pass through the arc, the NO_x yield would rise to 8.2% and the energy cost would drop to 0.5 MJ/mol NO_x, which would thus bring it close to the thermodynamic limit for plasma-based N_2 fixation (0.2 MJ/mol NO_x)[16]. This indicates that the GAP reactor is intrinsically very promising for N_2 fixation into NO_x, but the design will have to be modified, to enhance the fraction of gas passing through the arc. This reactor design modification and investigating the influence of heat recovery are planned for our future work. .

Conflicts of Interest

The authors declare that they have no known competing financial interests or personal relationships that could have appeared to influence the work reported in this paper.

Acknowledgements

This research was supported by the Excellence of Science FWO-FNRS project (FWO grant ID GoF9618n, EOS ID 30505023), the European Research Council (ERC) under the European Union's Horizon 2020 research and innovation programme (grant agreement No 810182 – SCOPE ERC Synergy project) and by a bilateral project with N2 Applied. The calculations were performed using

the Turing HPC infrastructure at the CalcUA core facility of the Universiteit Antwerpen (UAntwerpen), a division of the Flemish Supercomputer Center VSC, funded by the Hercules Foundation, the Flemish Government (department EWI) and the UAntwerpen.

Supporting Information

The Supporting Information contains: Literature overview table, details on the experimental setup, 0D model description, detailed experimental and modeling results, information on the Chi parameter, detailed reaction analysis, discussion of the VDFs of N_2 and O_2 and the full chemistry set including reaction rate constants.

REFERENCES

(1) Canfield, D. E.; Glazer, A. N.; Falkowski, P. G. The Evolution and Future of Earth's Nitrogen Cycle. *Science (80-.).* **2010**, *330* (6001), 192–196.

(2) Chanway, C. P.; Anand, R.; Yang, H. *Nitrogen Fixation Outside and inside Plant Tissues*; 2014.

(3) Bergman, B.; Sandh, G.; Lin, S.; Larsson, J.; Carpenter, E. J. Trichodesmium - a Widespread Marine Cyanobacterium with Unusual Nitrogen Fixation Properties. *FEMS Microbiol. Rev.* **2013**, *37* (3), 286–302.

(4) Kuypers, M. M. M.; Marchant, H. K.; Kartal, B. The Microbial Nitrogen-Cycling Network. *Nat. Rev. Microbiol.* **2018**, *16*, 263–276.

(5) Patil, B. S.; Wang, Q.; Hessel, V.; Lang, J. Plasma N 2 -Fixation : 1900 – 2014. *Catal. Today* **2015**, *256*, 49–66.

(6) Baltrusaitis, J. Sustainable Ammonia Production. *ACS Sustain. Chem. Eng.* **2017**, *5* (11), 9527.

(7) Cherkasov, N.; Ibhadon, A. O.; Fitzpatrick, P. A Review of the Existing and Alternative Methods for Greener Nitrogen Fixation. *Chem. Eng. Process. Process Intensif.* **2015**, *90*, 24–33.

(8) Patil, B. S.; Peeters, F. J. J.; van Rooij, G. J.; Medrano, J. A.; Gallucci, F.; Lang, J.; Wang, Q.; Hessel, V. Plasma Assisted Nitrogen Oxide Production from Air: Using Pulsed Powered Gliding Arc Reactor for a Containerized Plant. *AIChE J.* **2018**, *64* (2), 526–537.

(9) Gambarotta, S.; Scott, J. Multimetallic Cooperative Activation of N2. *Angew. Chemie - Int. Ed.* **2004**, *43* (40), 5298–5308.

(10) Chen, X.; Li, N.; Kong, Z.; Ong, W.-J.; Zhao, X. Photocatalytic Fixation of Nitrogen to Ammonia: State-of-the-Art Advancements and Future Prospects. *Mater. Horiz.* **2017**, *5* (1), 1–132.

(11) Wang, W.; Patil, B.; Heijkers, S.; Hessel, V.; Bogaerts, A. Nitrogen Fixation by Gliding Arc Plasma: Better Insight by Chemical Kinetics Modelling. *ChemSusChem* **2017**, *10* (10), 2110–2157.

(12) Birkeland, K. On the Oxidation of Atmospheric Nitrogen in Electric Arcs. *Trans. Faraday. Soc.* **1906**, *58*, 98–116.

(13) Hessel, V.; Cravotto, G.; Fitzpatrick, P.; Patil, B. S.; Lang, J.; Bonrath, W. Industrial Applications of Plasma, Microwave and Ultrasound Techniques: Nitrogen-Fixation and Hydrogenation Reactions. *Chem. Eng. Process. Process Intensif.* **2013**, *71*, 19–30.

(14) Patil, B. S. Plasma (Catalyst) – Assisted Nitrogen Fixation : Reactor Development for Nitric Oxide and Ammonia Production, Eindhoven University of Technology, 2017.

(15) Bogaerts, A.; Neyts, E. C. Plasma Technology: An Emerging Technology for Energy Storage. *ACS Energy Lett.* **2018**, *3* (4), 1013–1027.

(16) Rusanov, V. D.; Fridman, A. a.; Sholin, G. V. The Physics of a Chemically Active Plasma with Nonequilibrium Vibrational Excitation of Molecules. *Uspekhi Fiz. Nauk* **1981**, *134*, 449–472.

(17) Fridman, A. *Plasma Chemistry*; Intergovernmental Panel on Climate Change, Ed.; Cambridge University Press: Cambridge, 2005.

(18) Petitpas, G. Rollier, J. Darmon, A. Gonzalez-aguilar, J. Metkemeijer, R. Fulcheri, L. Comparative Study of Non-Thermal Plasma Assisted Reforming Technologies. *Int. J. Hydrogen Energy* **2007**, *32*, 2848–2867.

(19) Partridge, W. S.; Parlin, R. B.; Zwolinski, B. J. Fixation of Nitrogen in a Crossed Discharge. *Ind. Eng. Chem.* **1954**, *46*, 1468−1471.

(20) Bian, W; Song, X.; Shi, J.; Yin, X. Nitrogen Fixed into HNO3 by Pulsed High Voltage Discharge. *J. Electrostat* **2001**, *51–52*, 333–339.

(21) Coudert, J. F.; Baronnet, J. M.; Rakowitz, J.; Fauchais, P. Synthesis of Nitrogen Oxides in a Plasma Produced by a Jet Arc Generator. In *Symp. Int. Chim. Plasmas*; 1977.

(22) Rahman, M.; Cooray, V. NOx Generation in Laser-Produced Plasma in Air as a Function Ofdissipated Energy. *Opt. Laser Technol.* **2003**, *35*, 543–546.

(23) Mutel, B.; Dessaux, O.; Goudmand, P. Energy Cost Improvement Ofthe Nitrogen Oxides Synthesis in a Low Pressure Plasma. *Rev. Phys. Appl.* **1984**, *19*, 461–464.

(24) Polak, L. S.; Ovsiannikov, A. A.; Slovetsky, D. I.; Vurzel, F. B. *Theoretical and Applied Plasma Chemistry*; Nauka (Science): Moscow, 1975.

(25) Asisov, R. I.; Givotov, V. K.; Rusanov, V. D.; Fridman, A. No Title. *Sov. Phys. High Energy Chem (Khimia Vysok. Energ.* **1980**, *14*, 366.

(26) Patil, B. S.; Cherkasov, N.; Lang, J.; Ibhadon, A. O.; Hessel, V.; Wang, Q. Low Temperature Plasma-Catalytic NOxsynthesis in a Packed DBD Reactor: Effect of Support Materials and Supported Active Metal Oxides. *Appl. Catal. B Environ.* **2016**, *194* (2), 123–133.

(27) Malik, M. A.; Jiang, C.; Heller, R.; Lane, J.; Hughes, D.; Schoenbach, K. H. Ozone-Free Nitric Oxide Production Using an Atmospheric Pressure Surface Discharge - a Way to Minimize Nitrogen Dioxide Co-Production. *Chem. Eng. J.* **2016**, *283*, 631–638.

(28) Patil, B. S.; Rovira Palau, J.; Hessel, V.; Lang, J.; Wang, Q. Plasma Nitrogen Oxides Synthesis in a Milli-Scale Gliding Arc Reactor: Investigating the Electrical and Process Parameters. *Plasma Chem. Plasma Process.* **2016**, *36* (1), 241–257.

(29) Nunnally, T.; Gutsol, K.; Rabinovich, A.; Fridman, A.; Gutsol, A.; Kemoun, A. Dissociation of CO 2 in a Low Current Gliding Arc Plasmatron. *J. Phys. D. Appl. Phys.* **2011**, *44*, 274009–247016.

(30) Ramakers, M.; Trenchev, G.; Heijkers, S.; Wang, W.; Bogaerts, A. Gliding Arc Plasmatron: Providing an Alternative Method for Carbon Dioxide Conversion. *ChemSusChem* **2017**, *10* (12), 2642–2652.

(31) Ramakers, M. Heijkers, S. Tytgat, T. Lenaerts, S. Bogaerts, A. CO2 Conversion and N-Fixation Combined in a Gliding Arc Plasmatron. *J. CO2 Util.* **2019**, *33*, 121–130.

(32) Cleiren, E.; Heijkers, S.; Ramakers, M.; Bogaerts, A. Dry Reforming of Methane in a Gliding Arc Plasmatron: Towards a Better Understanding of the Plasma Chemistry. *ChemSusChem*

2017, *10* (20), 4025–4036.

(33) Trenchev, G.; Kolev, S.; Wang, W.; Ramakers, M.; Bogaerts, A. CO $_2$ Conversion in a Gliding Arc Plasmatron: Multidimensional Modeling for Improved Efficiency. *J. Phys. Chem. C* **2017**, *121* (44), 24470–24479.

(34) Trenchev, G.; Kolev, S.; Bogaerts, A. A 3D Model of a Reverse Vortex Flow Gliding Arc Reactor. *Plasma Sources Sci. Technol.* **2016**, *25* (3), 035014–035026.

(35) Heijkers, S.; Bogaerts, A. CO2Conversion in a Gliding Arc Plasmatron: Elucidating the Chemistry through Kinetic Modeling. *J. Phys. Chem. C* **2017**, *121* (41), 22644–22655.

(36) Gröger, S.; Hamme, M.; Bibinov, N.; Awakowicz, P.; Ramakers, M.; Bogaerts, A.; Medrano, J. A.; Gallucci, F. Characterization of a Nitrogen Gliding Arc Plasmatron Using Optical Emission Spectroscopy and High-Speed Camera. *J. Phys. D. Appl. Phys.* **2019**, *52* (6), 065201–065213.

(37) Ramakers, M.; Medrano, J. A.; Trenchev, G.; Gallucci, F.; Bogaerts, A. Revealing the Arc Dynamics in a Gliding Arc Plasmatron: A Better Insight to Improve CO2conversion. *Plasma Sources Sci. Technol.* **2017**, *26* (12), 125002–125014.

(38) Snoeckx, R.; Bogaerts, A. Plasma Technology – a Novel Solution for CO 2 Conversion? *Chem. Soc. Rev.* **2017**, 5805–5863.

(39) Kim, S. C.; Chun, Y. N. Development of a Gliding Arc Plasma Reactor for CO 2 Destruction. *Environ. Technol.* **2016**, *35*, 2940–2946.

(40) S. Pancheshnyi, B. Eismann, G.J.M. Hagelaar, L. C. P. Computer code ZDPlaskin http://www.zdplaskin.laplace.univ-tlse.fr.

(41) Heijkers, S.; Snoeckx, R.; Kozák, T.; Silva, T.; Godfroid, T.; Britun, N.; Snyders, R.; Bogaerts, A.

CO<inf>2</Inf> Conversion in a Microwave Plasma Reactor in the Presence of N<inf>2</Inf>: Elucidating the Role of Vibrational Levels. *J. Phys. Chem. C* **2015**, *119* (23), 12815–12828.

(42) Pei, X.; Gidon, D.; Yang, Y. J.; Xiong, Z.; Graves, D. B. Reducing Energy Cost of NO x Production in Air Plasmas. *Chem. Eng. J.* **2019**, *362* (x), 217–228.

(43) Murphy, A. B. Thermal Plasmas in Gas Mixtures. *J. Phys. D. Appl. Phys.* **2001**, *34*, R151–R173.

(44) Wang, W.; Rong, M.; Wu, Y.; Yan, J. D. Fundamental Properties of High-Temperature SF 6 Mixed with CO 2 as a Replacement for SF 6 in High-Voltage Circuit Breakers. *J. Phys. D. Appl. Phys.* **2014**, *47*, 255201–255217.

(45) Patel, H.; Sharma, R. K.; Kyriakou, V.; Pandiyan, A.; Welzel, S.; van de Sanden, M. C. M.; Tsampas, M. N. Plasma-Activated Electrolysis for Cogeneration of Nitric Oxide and Hydrogen from Water and Nitrogen. *ACS Energy Lett.* **2019**, *4*, 2091–2095.

(46) Wojciechowska, M.; Lomnicki, S. Nitrogen Oxides Removal by Catalytic Methods. *Clean Technol. Environ. Policy* **1999**, *1* (4), 237–247.

(47) Jin, Y.; Veiga, M. C.; Kennes, C. Bioprocesses for the Removal of Nitrogen Oxides from Polluted Air. *J. Chem. Technol. Biotechnol.* **2005**, *80* (5), 483–494.

(48) Poulton, B. B.; Foubert, L.; Klinowski, J.; Latimer, R. D.; Knowles, P. R.; Vuylsteke, A. Extraction of Nitric Oxide and Nitrogen Dioxide from an Oxygen Carrier Using Molecular Sieve 5A. *Br. J. Anaesth.* **1996**, *77* (4), 534–536.

(49) Triebe, R. W. T. F. H. R.W. Triebe. *Gas Sep. Purif.* **1995**, *9* (4), 223–230.

(50) Chang, M. B.; Lee, H. M.; Wu, F.; Lai, C. R. Simultaneous Removal of Nitrogen

Oxide/Nitrogen Dioxide/Sulfur Dioxide from Gas Streams by Combined Plasma Scrubbing Technology. *J. Air Waste Manag. Assoc.* **2004**, *54* (8), 941–949.

Synopsis

0D modeling provides insight into N_2/O_2 plasma chemistry, allowing us to pinpoint and subsequently improve NO_X formation in a gliding arc plasmatron.